Phys Chem Minerals (2003) 30: 192–197
DOI 10.1007/s00269-003-0308-4

ORIGINAL PAPER

R. Hellmann · J.-M. Penisson · R. L. Hervig
J.-H. Thomassin · M.-F. Abrioux

An EFTEM/HRTEM high-resolution study of the near surface of labradorite feldspar altered at acid pH: evidence for interfacial dissolution-reprecipitation

Received: 31 October 2002 / Accepted: 14 February 2003

Abstract Using an approach combining high-resolution and energy-filtered transmission electron microscopy (HRTEM and EFTEM), we have studied with Å to nm-spatial resolution the interfacial region that delimits the near-surface altered zone and non-altered labradorite feldspar after dissolution under acid pH conditions. The interface is characterized by extremely sharp and spatially coincident changes in structure and chemistry. The 500-nm-thick altered zone is depleted in interstitial cations (Ca, Na, K) and Al, a framework element, whereas it is enriched in H, O, and Si. Modeling H^+-alkali interdiffusion within a 500-nm-thick altered zone shows that volume interdiffusion cannot reproduce the sharp chemical interfaces measured by EFTEM. Based on these new data, we propose that the near-surface altered zone is a result of interfacial dissolution-reprecipitation, and not of preferential leaching of cations and interdiffusion with H^+. This implies an intrinsic dissolution process that is stoichiometric, where the breaking of bonds and release of interstitial cations and framework elements (Al, Si, and O) to solution occur contemporaneously at equal relative rates from the original fluid–mineral interface.

Keywords Feldspar dissolution · EFTEM and HRTEM · Interfacial dissolution – reprecipitation mechanism · Leached layers and preferential cation release

R. Hellmann (✉)
LGIT, CNRS UMR C5559-OSUG-Université
J. Fourier, 38041 Grenoble Cedex 9, France
e-mail: hellmann@obs.ujf-grenoble.fr

J.-M. Penisson
DRFMC, CEA-Grenoble, 38054 Grenoble Cedex 9, France

R. L. Hervig
Center for Solid State Science, Arizona State University,
Tempe, Arizona 85287–1704, USA

J.-H. Thomassin · M.-F. Abrioux
UMR CNRS 6532, LMGE – ESIP- Université de Poitiers,
86022 Poitiers Cedex, France

Introduction

Prevailing dissolution models postulate that feldspars dissolve via two separate, pH-dependent mechanisms: nonstoichiometric dissolution (preferential element release) and near-surface alteration at acid to neutral pH, and stoichiometric dissolution and absence of near-surface alteration at basic pH (e.g. Chou and Wollast 1985; Holdren and Speyer 1985; Nesbitt and Muir 1988; Casey et al. 1989a,b; Petit et al. 1989; Hellmann et al. 1990; Petit et al. 1990a,b; Hellmann 1995; Schweda et al. 1997; Nugent et al. 1998). Nonstoichiometric dissolution results in the development of chemically and structurally altered near-surface zones (commonly called leached layers) between the fluid–solid interface and the unaltered mineral matrix (e.g., Nesbitt and Muir 1988; Casey et al. 1989a,b; Petit et al. 1989; Hellmann et al. 1990; Petit et al. 1990a,b; Schweda et al. 1997). These altered zones are different and spatially distinct from secondary crystalline phases, such as metal (oxy)hydroxides and clays, that may precipitate on mineral surfaces during dissolution (e.g. Nugent et al. 1998). Leached layers are generally not observed at basic pH. This feldspar dissolution model is commonly applied to other aluminosilicate minerals that also display non-stoichiometric, pH-dependent alteration (e.g. Petit et al. 1990a,b; Casey et al. 1993; Weissbart and Rimstidt 2000).

Depth profiles of altered near-surface zones (leached layers) developed on acid to neutral pH-dissolved feldspars, based on surface-sensitive spectroscopic (e.g. Hochella et al. 1988; Hellmann et al. 1990; Muir et al. 1990; Inskeep et al. 1991; Gout et al. 1997; Chen et al. 2000; Nesbitt and Skinner 2001) and ion beam techniques (e.g. Nesbitt and Muir 1988; Casey et al. 1989a; Petit et al. 1989; Petit et al. 1990a,b; Muir et al. 1990; Hellmann et al. 1997; Muir and Nesbitt 1997; Schweda et al. 1997), typically show depletion of interstitial cations (Na, K, Ca) and certain framework elements (Al), retention of Si and O, and enrichment in aqueous species, most notably H. The leached layer hypothesis

postulates that preferential cation leaching and H incorporation result in the formation of a relic structure bounded by fluid on one side and by the unaltered matrix on the other. The role of interdiffusion in the formation of leached layers is supported by anticorrelated, sigmoidal depth profiles of depleted and enriched elements that have been measured by various ion beam and spectroscopy techniques (e.g. Casey et al. 1989a; Petit et al. 1989; Hellmann et al. 1990; Petit et al. 1990b; Schweda et al. 1997).

In this study we examined labradorite feldspar that was altered at room temperature at pH 1; low pH conditions were chosen to ensure thick altered zones suitable for study. Instead of exclusively obtaining depth profiles using ion beam techniques that are incident to the original surface, we used an ultramicrotome technique to prepare electron-transparent thin sections, such that the altered zones could be studied in cross-section. The physical and chemical nature of the interfacial boundary between near-surface altered zones and unaltered matrix was examined in detail using both high-resolution and energy-filtered transmission electron microscopy (HRTEM and EFTEM, respectively). This approach has allowed us to obtain a unique combination of chemical and structural information at Å- to nm-scale spatial resolution which is significantly higher than in previous studies. In addition to the aforementioned techniques, secondary ion mass spectrometry (SIMS) was used to obtain chemical profiles of the altered zones (especially useful for H). Our combined HRTEM, EFTEM, and SIMS data on acid pH-altered labradorite feldspar are consistent with a different mechanism of dissolution, one that is based on interfacial dissolution-reprecipitation.

Experimental

Sample preparation

Samples of labradorite feldspar ($Na_{0.39}Ca_{0.59}Al_{1.59}Si_{2.41}O_8$) were cut from clear crystals into $10 \times 10 \times 5$ mm wafers, polished with diamond paste to 0.1 μm, and cleaned in acetone. Samples were dissolved in a HCl/H_2O solution at pH 1 (500 h) at 22 ± 2 °C in a flowthrough reactor ($V = 50$ ml). The reacted samples used in this study were provided by P. Schweda (for more details, see Schweda et al. 1997). The chemistry of the reacted (output) solutions was below standard analytical limits (P. Schweda, personal communication, 2001). Postreaction samples were gold-coated, and several of these samples were then prepared in cross-section by an ultramicrotome; the protocol involves multiple steps of epoxy impregnation, sample extraction, and microsawing, followed by slicing of the sample with a diamond knife in an ultramicrotome, this producing numerous electron-transparent ultrathin sections. These were then deposited on a holey carbon film-coated TEM grid for subsequent analysis by HRTEM and EFTEM.

Instrumental analyses

We used a Jeol 3010 TEM (CEA) operated at 300 kV with a point resolution of 0.17 nm to obtain Å-resolution structural images of the interfacial structure. EFTEM jump ratio images and electron energy loss spectroscopy (EELS) spectra were obtained with a Gatan imaging filter attached to a JEOL 3010 TEM (CEA) operated at 300 keV, energy dispersion = 0.2 eV channel^{-1}, and collection angle ß = 6.5 mrad. In this study we used the Ca $L_{2,3}$, O K, Al K, and Si K edges. Each jump ratio image was calculated by dividing the post-edge image by the pre-edge image (see details in Hofer et al. 1997). The pre- and post-edge images were based on a 20–30-eV-wide energy window slightly before and after the core-loss ionization edge (the optimum width and position were based on values provided by Gatan's Digital Micrograph software, with the exception of Ca $L_{2,3}$ images, where a larger energy window was chosen). SIMS profiles were obtained with a Cameca IMS 3f instrument (ASU) using an $^{16}O^-$ primary ion beam with the following instrument settings: 25 nA beam current, 12.6 kV accelerating voltage, 125×125 μm^2 raster area, ion beam incident at 30° to sample normal (with respect to original Au-coated surface).

Results

Examination of numerous ultramicrotome-thin sections of labradorite dissolved at pH 1 with conventional transmission electron microscopy (TEM) shows that the altered zone is 500 nm thick, with an interface between the amorphous altered zone and crystalline labradorite that is notably sharp. This is consistent with other studies of acid pH-altered feldspars and other aluminosilicates where sharp structural interfaces have been documented (e.g. Figs. 6, 1, 3 in Casey et al. 1989a,b, 1993, respectively – note that the resolution of these images is not sufficient to exactly quantify the interfacial widths). To characterize the exact nature of the interface at Å resolution, we examined the interfacial boundary between altered and nonaltered zones by HRTEM. The amorphous–crystalline interface is locally linear and atomically sharp, with a width varying between 0.5–2 nm (Fig. 1). The interface appears to have a variable width because it is affected

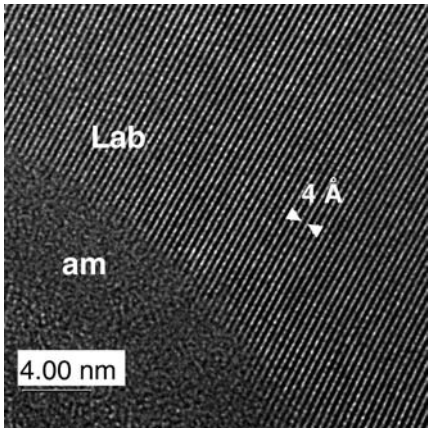

Fig. 1 Ultrathin section of labradorite feldspar altered at pH 1. HRTEM image of interface (thickness ≈ 0.5 to 2 nm) that delimits the amorphous altered zone (*bottom left*) and crystalline unaltered labradorite (*top right*). The interface appears to have a variable width (i.e. note blurry lattice fringes at interface, *bottom of image*) because it is affected by nonconstant orientation of the interfacial boundary with respect to the surface of the ultrathin section and the incoming electron beam

by nonconstant orientation of the interfacial boundary with respect to the surface of the ultrathin section and the incoming electron beam.

Chemical depth profiles measured by SIMS reveal that the altered zone is depleted in the interstitial cations Ca, Na and K, as well as in Al, a framework element; it is enriched in H, O, Si, and B (boron was present as an impurity in the aqueous solutions). Our SIMS results are in good accord with previous SIMS and other ion beam and spectroscopy measurements of acid pH-altered near-surface zones on feldspars (e.g. Casey et al. 1989a; Hellmann et al. 1990; Inskeep et al. 1991; Muir and Nesbitt 1997; Schweda et al. 1997; Nesbitt and Skinner 2001). Detailed SIMS profiles obtained from labradorite samples altered at pH 1, 2, and 3 are presented in an upcoming study (R. Hellmann et al., in preparation).

Using the same ultramicrotome-thin sections studied by HRTEM, we examined the chemistry of the interfacial region by EFTEM, a method that provides a 2-D spatial distribution (i.e. concentration map) of any given element (H, He excluded) at nm resolution. EFTEM jump-ratio images of a typical interfacial region portray qualitatively the concentrations of Ca, Al, Si, and O (Fig. 2a). The most important point to note in this figure is that the sharp, step-like changes in the concentrations of these four elements (Fig. 2a) occur exactly at the same interfacial boundary that marks the structural transition between the amorphous, altered zone and the unaltered, crystalline labradorite (Fig. 2b). Chemical profiles across and perpendicular to the interfacial region (see insets, Fig. 2a) give the following interfacial boundary thicknesses (in nm): Ca $\approx$ 3.8; Al $\approx$ 5.1; Si $\approx$ 6.8; O $\approx$ 4.9. Note also that the four separate chemical maps in Fig. 2a confirm the SIMS results: depletion of Ca and Al, and enrichment of O and Si in the altered zone. The difference in the thickness of the interfacial boundary as

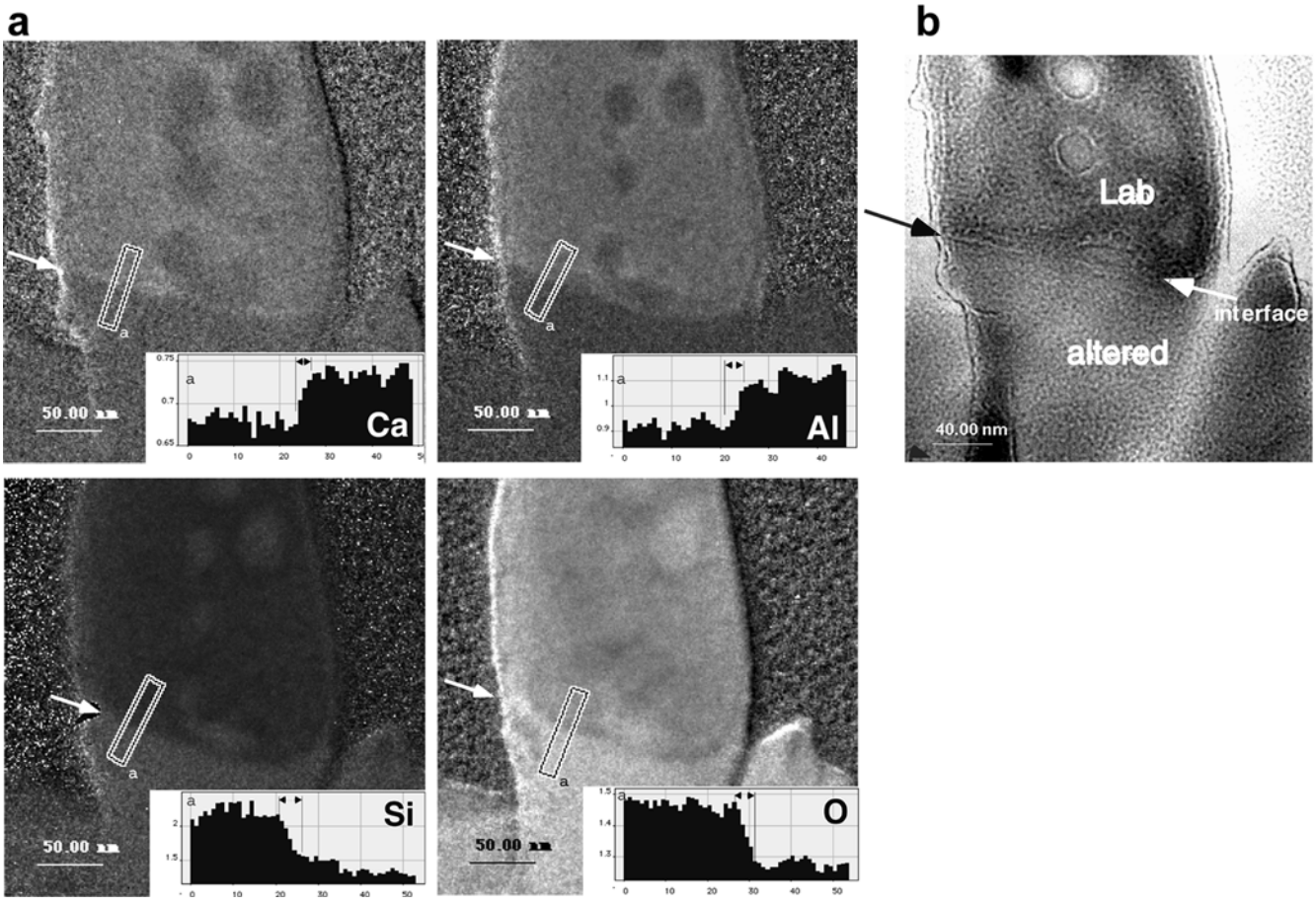

Fig. 2a, b Ultrathin section lamella of labradorite feldspar altered at pH 1 showing the interface between the altered zone (*bottom*) and the unaltered labradorite (*top*); note the exact spatial coincidence between chemical interfaces in **a** and structural interface in **b**. The lamellar nature of the thin section is an artefact of the ultramicrotome technique. **a** EFTEM chemical maps of the interfacial boundary (*white arrows*) separating the altered and unaltered zones; qualitative concentrations of Ca, Al, Si and O shown (brightness proportional to concentration). Calcium and Al are depleted in the altered zone, whereas Si and O are enriched. *Insets* show the respective chemical profiles (*left to right* from altered to nonaltered zones); delimiting *small black arrows in insets* indicate estimated widths of interfacial regions (note: abscissa axes are in pixels, 1 pixel = 1.26 nm; ordinate axes have arbitrary units). The chemical gradients are very sharp, ranging from $\approx$3.8 nm (Ca) to 6.8 nm (Si). **b** Zero-loss image, showing interface (*arrows*) between amorphous altered zone and crystalline unaltered labradorite. The irregular, subround regions visible in **a** and **b** are due to electron beam damage. The four EFTEM images in **a** show an EFTEM-jump ratio artefact (due to instrument drift or electrical charging of the specimen) that results in a white and dark fringe on the *left and right side* of each lamella – the actual chemical gradients may therefore be even sharper than reported

measured by HRTEM and EFTEM is most probably a function of the lower inherent resolution of the EFTEM technique. An EFTEM-image artefact (see caption, Fig. 2) may also be responsible for a slight decrease in the resolution.

Discussion

Interdiffusion modeling

Modeling simultaneously steady-state dissolution and binary interdiffusion allows us to test whether the sharp interfacial chemical gradients that were measured by EFTEM (Fig. 2a) can be formed by the leached layer mechanism. We used the following expression, which has been applied to interdiffusion in altered glasses (Doremus 1975) and is based on a semi-infinite geometry and constant concentration at the fluid–solid interface

$$\left(\frac{\partial C}{\partial t}\right) = \frac{\partial}{\partial x}\left(\tilde{D}\frac{\partial C}{\partial x}\right) + a\left(\frac{\partial C}{\partial x}\right) = 0. \quad (1)$$

In the above equation, C is the normalized concentration of the element chosen, x is the depletion or enrichment depth (measured from the fluid–solid interface), $\tilde{D}$ is an interdiffusion coefficient, a is the rate of retreat of the fluid–solid interface, and because steady-state conditions were assumed, $\partial C/\partial t = 0$. To compare the EFTEM results with the interdiffusion model given in Eq. (1), parameters corresponding to labradorite dissolution at 22 °C and pH 1 were used. In particular, the rate of retreat of the fluid–solid interface a was calculated from two parameters: previously measured dissolution rates from Oxburgh et al. (1994) and the molar volume from Schweda et al. (1997) and Smith and Brown (1988).

The diffusion process that we examine is based on binary interdiffusion (Baucke 1974; Doremus 1975) of H^+ and an alkali cation (note that below we use "alkali" and "cation" interchangeably). A single interdiffusion coefficient $\tilde{D}$ is used to describe their mutual interdiffusion behavior (Darken 1948; Hartley and Crank 1949)

$$\tilde{D} = \frac{D_H}{1 + bC_H}, \quad (2)$$

where $b = (D_H/D_{alk}) - 1$.

The values of $\tilde{D}$ are based on the assumption that $D_H < D_{alk}$, in accord with H and alkali diffusive mobilities that have been measured during the aqueous alteration of glasses (Baucke 1974; Lanford et al. 1979; Smets and Lommen 1982; and references therein). The mathematical form of $\tilde{D}$ satisfies the condition that the altered zone is structurally contiguous with the unaltered mineral at their mutual interface.

Substitution of Eq. (2) into Eq. (1) and integrating twice with the appropriate boundary conditions (see Hellmann 1997 for details) allows one to portray C_{alk} and C_H vs. depth x. Figure 3 illustrates H and cation

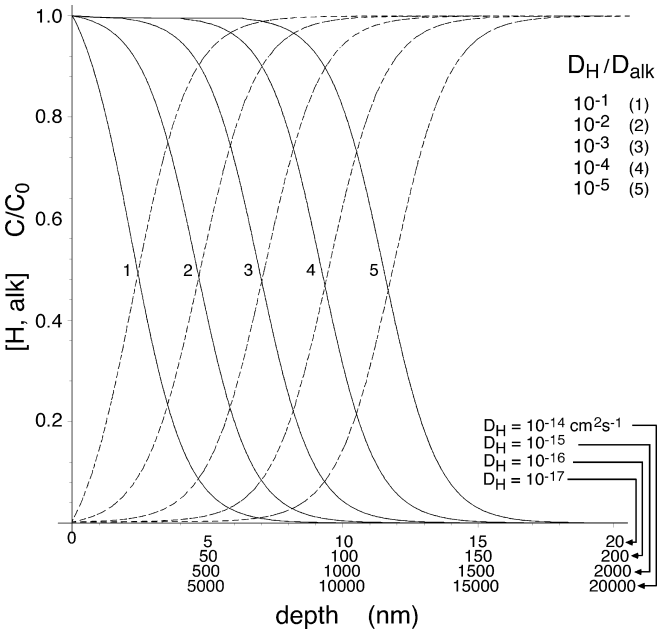

Fig. 3 Interdiffusion profiles of alkali cations and H^+ based on Eqs. (1) and (2) (see text). Note that the depth of H penetration/cation depletion is largely controlled by D_H. The interfacial thickness of a given profile (width of sigmoidal part of profile) is directly related to the depth of H penetration/cation depletion. These interdiffusion profiles do not reproduce the EFTEM results, namely a 500-nm-thick altered zone with nm-wide interfacial chemical gradients

interdiffusion profiles, based on $D_H = 10^{-17}$, 10^{-16}, 10^{-15}, 10^{-14} cm^2 s^{-1}, and $D_H/D_{alk} = 10^{-1}$–10^{-5} for each respective value of D_H. The anticorrelated, sigmoidal nature of the profiles is a characteristic of diffusion fronts associated with interdiffusion. The depths of H penetration and cation depletion can be assigned to the inflection point of a particular set of anticorrelated sigmoidal profiles (i.e. the depth at half-height); the interfacial thickness corresponds to the width of the sigmoidal part of a given profile.

Figure 3 illustrates that the depths of H penetration and cation depletion are very sensitive to D_H, whereas much less so to D_{alk}. The thickness of the interfacial gradient is also strongly dependent on D_H, and much less on D_{alk}. The interdiffusion profiles in Fig. 3 demonstrate two important points: (1) the depth of H penetration and cation depletion is largely controlled by D_H; (2) the interfacial thickness is directly related to the depth of H penetration/cation depletion. The latter point is important to our argument, that is the interdiffusion model we use can produce chemical profiles that have thin, nm-wide interfacial gradients, but only in conjunction with extremely shallow depths of H penetration and cation depletion.

The depths of H penetration and cation depletion that were measured by SIMS and EFTEM in this study correspond most closely to the theoretical interdiffusion profiles governed by $D_H = 10^{-15}$ cm^2 s^{-1} and $D_H/D_{alk} = 10^{-2}$ in Fig. 1 (profile 2). On the other hand, these anticorrelated profiles have an interfacial thickness of

≈900 nm, which is 2 orders of magnitude greater than those measured by EFTEM (Fig. 2a). Therefore, based on the results shown in Fig. 3, the interdiffusion model given by Eq. (1) when combined with an interdiffusion coefficient given by Eq. (2) is not capable of reproducing both H penetration/cation depletion profiles with a depth on the order of 500 nm, as well as nm-wide interfacial gradients.

The model we have presented is based on a simple interdiffusion process, one that has been successfully applied to the study of glass alteration (e.g. Doremus 1975; Lanford et al. 1979). Not surprisingly, other diffusion models based on various interdiffusion coefficients also fail to reproduce diffusion fronts with nm-wide chemical gradients (R. Hellmann et al., in preparation). Taken together, these results suggest that the measured EFTEM profiles are not due to a volume interdiffusion process.

Interfacial dissolution-reprecipitation mechanism

We argue that the altered zones that we observed form via a process that we term interfacial dissolution-reprecipitation. Such a mechanism is compatible with our high-resolution data, in particular the abrupt amorphous-crystalline structural transition (0.5–2Å) combined with the very sharp, nm-wide chemical gradients at the altered zone–mineral interface. We stress that this mechanism is interfacial in nature: bond-breaking and element release, followed by reprecipitation, occur directly at the original fluid–mineral interface. The observed altered zone can now be understood in terms of the reprecipitation of an amorphous secondary phase that results in a sharp (Å to nm-wide) structural and chemical interface with the dissolving mineral interface. Being composed primarily of Si, O, and H, the interfacial precipitate most likely is a hydrated silica gel (Murata 1943; Teng et al. 2001). Based on BET measurements of acid pH-altered plagioclase by Casey et al. (1989b), the altered zone is very porous and should therefore be very permeable to fluids, ensuring nondiffusion-limited transport of elements through the gel layer (i.e. diffusion rates comparable to those in a fluid). Therefore, the gel layer should not affect the rate of the intrinsic dissolution process.

Several published studies are compatible with our data and appear to support our ideas. For example, recent X-ray reflectivity data were interpreted by Fenter et al. (2000) to show that exchange of H species with interstitial K on orthoclase feldspar altered at neutral pH is limited to the topmost K layer. Using the same technique, Teng et al. (2001) presented evidence that orthoclase dissolution at acid pH is only minimally nonstoichiometric, suggesting that H^+–K^+ exchange is limited to one unit-cell depth. Our model also has many similarities with very sharp chemical and isotopic gradients that have been measured at the interface between feldspar phases undergoing "cation exchange" reactions under hydrothermal conditions (O'Neil and Taylor 1967; Fiebig and Hoefs 2002; Labotka et al. 2002).

At this point we need to distinguish our model from another mechanism often cited in the dissolution literature, namely hydrolysis-recondensation. This mechanism has frequently been presented as an integral part of the leached layer model, where it is postulated to structurally stabilize leached layers formed during glass (e.g. Bunker et al. 1988; Bunker 1994) and aluminosilicate mineral alteration (e.g. Casey et al. 1989a,b, 1993). Nonetheless, this latter mechanism is based on hydrolysis and recondensation (polymerization) reactions that occur within leached layers that owe their existence to the initial preferential release of certain cations and interdiffusion with H^+; it is thus incompatible and quite different from the interfacial dissolution-reprecipitation model we propose.

Conclusions

Even though our study only presents data concerning labradorite reacted at pH 1, we can speculate much further on the potential importance of our results. If our model for intrinsic stoichiometric dissolution is found to hold for all feldspars (orthoclase, albite, plagioclases) over the entire acid to neutral pH range, then this would imply that the intrinsic feldspar dissolution process (i.e. bond-breakage and release of elements) under these pH conditions operates in a manner similar to what has always been observed at basic pH, that is stoichiometric dissolution (e.g. Chou and Wollast 1985; Holdren and Speyer 1985). This would suggest a single, pH-invariant surface release mechanism which ensures that the relative release rates of all surface constituents (interstitial cations and framework elements) are equal and contemporaneous, and that bond-breakage and detachment occur from the same fluid–mineral interface. It is important to note, however, that our proposed stoichiometric and pH-invariant mechanism does not imply that the overall dissolution process is pH-independent, as the overall rates of release are obviously very pH-dependent.

When bulk solution analyses of feldspar dissolution experiments or weathering in natural environments are measured, deviations from stoichiometric dissolution behavior at acid to neutral pH conditions can now be thought of in a different manner, and should be attributed (at least in part) to interfacial reprecipitation of a silica gel that occurs immediately after the initial, stoichiometric detachment of constituent elements from the feldspar surface. This process may occur simultaneously with the bulk precipitation of crystalline secondary phases, a phenomenon that is commonly observed in naturally weathered feldspars (e.g. Nugent et al. 1998). Thus, depending on the exact chemistry of the fluid and its evolution with time, the fluid–solid interface of a dissolving feldspar can be thought of as a sandwich, composed of a potentially thick outer layer (in the range

of μm to mm) of clays and/or metal oxy-hydroxides that have precipitated on top of a hydrated silica gel, which, in turn, covers the stoichiometrically dissolving, original feldspar surface.

Acknowledgements This study was financed (in part) by the Centre National de la Recherche Sciéntifique (CNRS) and Agence nationale pour la gestion des déchets radioactifs (ANDRA) through GdR FORPRO (research action number 99.3) and corresponds to GdR FORPRO contribution number 2002/05 A. Funding to R. Hervig from the US Dept. of Energy, grant DE FG05 97ER14414. We thank P. Schweda for providing us with the reacted samples of labradorite.

References

Baucke FGK (1974) Investigation of surface layers, formed on glass electrode membranes in aqueous solutions, by means of an ion sputtering method. J Non-Crystal Solids 14: 13–31

Bunker BC (1994) Molecular mechanisms for corrosion of silica and silicate glasses. J Non-Crystal Solids 179: 300–308

Bunker BC, Tallant DR, Headley TJ, Turner GL, Kirkpatrick RJ (1988) The structure of leached sodium silicate glass. Phys Chem Glasses 29: 106–120

Casey WH, Westrich HR, Arnold GW, Banfield JF (1989a) The surface chemistry of dissolving labradorite feldspar. Geochim Cosmochim Acta 53: 821–832

Casey WH, Westrich HR, Massis T, Banfield JF, Arnold GW (1989b) The surface of labradorite feldspar after acid hydrolysis. Chem Geol 78: 205–218

Casey WH, Westrich HR, Banfield JF, Ferruzzi G, Arnold GW (1993) Leaching and reconstruction at the surfaces of dissolving chain-silicate minerals. Nature 366: 253–255

Chen Y, Brantley SL, Ilton ES (2000) X-ray photoelectron spectroscopic measurement of the temperature dependence of leaching of cations from the albite surface. Chem Geol 163: 115–128

Chou L, Wollast R (1985) Steady-state kinetics and dissolution mechanisms of albite. Am J Sci 285: 963–993

Darken LS (1948) Diffusion, mobility, and their interrelation through free energy in binary metallic systems. Am Inst Min Metal Engrs Trans 175: 184–201

Doremus RH (1975) Interdiffusion of hydrogen and alkali ions in a glass surface. J Non-Crystal Solids 19: 137–144

Fenter P, Teng H, Geissbühler P, Hanchar JM, Nagy KL, Sturchio NC (2000) Atomic-scale structure of the orthoclase (001)–water interface measured with high-resolution X-ray reflectivity. Geochim Cosmochim Acta 64: 3663–3673

Fiebig J, Hoefs J (2002) Hydrothermal alteration of biotite and plagioclase as inferred from intragranular oxygen isotope- and cation-distribution patterns. Eur J Mineral 14: 49–60

Gout R, Oelkers EH, Schott J, Zwick A (1997) The surface chemistry and structure of acid-leached albite. New insights on the dissolution mechanism of the alkali feldspars. Geochim Cosmochim Acta 61: 3013–3018

Hartley GS, Crank J (1949) Some fundamental definitions and concepts in diffusion processes. Trans Faraday Soc 45: 801–818

Hellmann R (1995) The albite–water system, part II. The time evolution of the stoichiometry of dissolution as a function of pH at 100, 200 and 300 °C. Geochim Cosmochim Acta 59: 1669–1697

Hellmann R (1997) The albite–water system part IV. Diffusion modeling of leached and hydrogen-enriched layers. Geochim Cosmochim Acta 61: 1595–1611

Hellmann R, Eggleston CM, Hochella MF Jr, Crerar DA (1990) The formation of leached layers on albite surfaces during dissolution under hydrothermal conditions. Geochim Cosmochim Acta 54: 1267–1281

Hellmann R, Dran J-C, Della Mea G (1997) The albite–water system, part III. Characterization of leached and hydrogen-enriched layers formed at 300 °C using MeV ion beam techniques. Geochim Cosmochim Acta 61: 1575–1594

Hochella MF Jr, Ponader HB, Turner AM, Harris DW (1988) The complexity of mineral dissolution as viewed by high-resolution scanning Auger microscopy: labradorite under hydrothermal conditions. Geochim Cosmochim Acta 52: 385–394

Hofer F, Grogger W, Kothleitner G, Warbichler P (1997) Quantitative analysis of EFTEM elemental distribution images. Ultramicroscopy 67: 83–103

Holdren GR Jr, Speyer PM (1985) pH dependent changes in the rates and stoichiometry of dissolution of an alkali feldspar at room temperature. Am J Sci 285: 994–1026

Inskeep WP, Nater EA, Bloom PR, Vandervoort DS, Erich MS (1991) Characterization of laboratory-weathered labradorite surfaces using X-ray photoelectron spectroscopy and transmission electron microscopy. Geochim Cosmochim Acta 55: 787–800

Labotka T, Cole DR, Fayek M, Riciputi LR (2002) Coupled cation and oxygen exchange between alkali feldspar and aqueous chloride solution. Geochim Cosmochim Acta 66: A427 (Abstr.)

Lanford WA, Davis K, Lamarche P, Laursen T, Groleau R (1979) Hydration of soda-lime glass. J Non-Crystal Solids 33: 249–266

Muir IJ, Nesbitt HW (1997) Reactions of aqueous anions and cations at the labradorite–water interface: coupled effects of surface processes and diffusion. Geochim Cosmochim Acta 61: 265–274

Muir IJ, Bancroft GM, Shotyk W, Nesbitt HW (1990) A SIMS and XPS study of dissolving plagioclase. Geochim Cosmochim Acta 54: 2247–2256

Murata KJ (1943) Internal structure of silicate minerals that gelatinize with acid. Am Mineral 28: 545–562

Nesbitt HW, Muir IJ (1988) SIMS depth profiles of weathered plagioclase, and processes affecting dissolved Al and Si in some acidic soil conditions. Nature 334: 336–338

Nesbitt HW, Skinner WM (2001) Early development of Al, Ca, and Na compositional gradients in labradorite leached in pH 2 HCl solutions. Geochim Cosmochim Acta 65: 715–727

Nugent MA, Brantley SL, Pantano CG, Maurice PA (1998) The influence of natural mineral coatings on feldspar weathering. Nature 395: 588–591

O'Neil JR, Taylor HPJ (1967) The oxygen isotope and cation exchange chemistry of feldspars. Am Mineral 52: 1414–1437

Oxburgh R, Drever JI, Sun Y-T (1994) Mechanism of plagioclase dissolution in acid solution at 25 °C. Geochim Cosmochim Acta 58: 661–669

Petit J-C, Dran J-C, Paccagnella A, Della Mea G (1989) Structural dependence of crystalline silicate hydration during aqueous dissolution. Earth Planet Sci Lett 93: 292–298

Petit J-C, Della Mea G, Dran J-C, Magonthier M-C, Mando PA, Paccagnella A (1990a) Hydrated layer formation during dissolution of complex silicate glasses and minerals. Geochim Cosmochim Acta 54: 1941–1955

Petit J-C, Dran J-C, Della Mea G (1990b) Energetic ion beam analysis in the Earth sciences. Nature 344: 621–626

Schweda P, Sjöberg L, Södervall U (1997) Near-surface composition of acid-leached labradorite investigated by SIMS. Geochim Cosmochim Acta 61: 1985–1994

Smets BMJ, Lommen TPA (1982) The leaching of sodium aluminosilicate glasses studied by secondary ion mass spectrometry. Phys Chem Glasses 23: 83–87

Smith JV, Brown WL (1988) Feldspar minerals 1. Crystal structures, physical, chemical and microtextural properties feldspar minerals. Springer, Berlin, Heidelberg New York

Teng HH, Fenter P, Cheng L, Sturchio NC (2001) Resolving orthoclase dissolution processes with atomic force microscopy and X-ray reflectivity. Geochim Cosmochim Acta 65: 3459–3474

Weissbart EJ, Rimstidt JD (2000) Wollastonite: incongruent dissolution and leached layer formation. Geochim Cosmochim Acta 64: 4007–4016